Probing the global potential energy minimum of $(CH_2O)_2$: THz absorption spectrum of $(CH_2O)_2$ in solid neon and para-hydrogen

Andersen, Jonas; Voute, A.; Mihrin, Dmytro; Heimdal, Jimmy; Berg, Rolf W.; Torsson, M. ; Larsen, René Wugt

Published in:
Journal of Chemical Physics

Link to article, DOI:
10.1063/1.4990042

Publication date:
2017

Document Version
Peer reviewed version

Probing the Global Potential Energy Minimum of $(CH_2O)_2$: THz Absorption Spectrum of $(CH_2O)_2$ in Solid Neon and Para-Hydrogen

J. Andersen, A. Voute, D. Mihrin, J. Heimdal,
R. W. Berg, M. Torsson and R. Wugt Larsen*

Department of Chemistry, Technical University of Denmark, Kemitorvet 206, 2800 Kgs. Lyngby, Denmark

May 14, 2017

The true global potential energy minimum configuration of the formaldehyde dimer $(CH_2O)_2$, including the presence of a single or a double weak intermolecular CH··O hydrogen bond motif, has been a long-standing subject among both experimentalists and theoreticians as two different energy minima conformations of C_s and C_{2h} symmetry have almost identical energies. The present work demonstrates how the class of large-amplitude hydrogen bond vibrational motion probed in the THz region provides excellent *direct* spectroscopic observables for these weak intermolecular CH··O hydrogen bond motifs. The combination of concentration dependency measurements, observed isotopic spectral shifts associated with H/D substitutions and dedicated annealing procedures enables the unambiguous assignment of three large-amplitude infrared active hydrogen bond vibrational modes for the non-planar C_s configuration of $(CH_2O)_2$ embedded in cryogenic neon and enriched para-hydrogen matrices. A (semi)-empirical value for the change of vibrational zero-point energy of 5.5±0.3 kJ·mol^{-1} is proposed for the dimerization process. These THz spectroscopic observations are complemented by CCSD(T)-F12/aug-cc-pV5Z (electronic energies) and MP2/aug-cc-pVQZ (force fields) electronic structure calculations yielding a (semi)-empirical value of 13.7±0.3 kJ·mol^{-1} for the dissociation energy D_0 of this global potential energy minimum.

*Corresponding Author: rewl@kemi.dtu.dk

1. Introduction

Hydrogen bonding is a concept of enormous importance for a vast number of phenomena within diverse scientific areas e.g. the anomalous thermodynamic behavior of condensed phases, the mechanical properties of functional materials and the complex molecular recognition of biological macromolecules. In a modern context, the concept of hydrogen bonding is understood as a complex phenomenon spanning two order of magnitudes in the range from about 0.2 to 40 kcal·mol^{-1}.[1] The nature of weak hydrogen bond interactions such as CH··O and OH··π contacts are typically dominated by electrostatic and London dispersion contributions alone, making a clear-cut distinction between weak hydrogen bonds and strict non-covalent van der Waals interactions rather challenging. In terms of reliable quantum chemical methodologies, both high levels of electron correlation, extensive basis sets and the inclusion of basis set superposition errors and anharmonic vibrational zero-point energy contributions have proven mandatory to accurately predict the geometrical and energetical characteristics of these weak hydrogen bond interactions. A reliable experimental detection of this class of weak non-covalent interactions on the other hand, requires sensitive and unambiguous spectroscopic observables which are not blurred by thermal broadening, crystal-field effects and chemical inhomogeneities. An accurate characterization of weak hydrogen bonding motifs cannot be extracted directly from crystalline phases and the reductionistic approach is then to experimentally investigate relevant isolated molecular model systems which are amendable for high-level quantum chemical methods within the "supermolecule" approach. The simplest suitable representative for this "supermolecule" approach involving weak intermolecular CH··O hydrogen bonding is the homodimer of formaldehyde, $(CH_2O)_2$. The specific non-covalent forces at play in this prototypical dimerization recognition process have been the subject of a wealth of theoretical and experimental investigations over the last two decades.

The first experimental investigation of $(CH_2O)_2$ embedded in argon and nitrogen matrices was reported by Khoshkhoo and Nixon.[2] Based on combined infrared and Raman observations for the perturbed intramolecular C=O stretching modes, these authors concluded that $(CH_2O)_2$ must have a center of symmetry. Subsequently, a nitrogen matrix isolation study by Nelander[3] and a pulsed-nozzle Fourier transform microwave study by Lovas et *al.*[4] both suggested that the two subunits are equivalent in the dimer consistent with a C_s potential energy minimum without a center of symmetry. From a theoretical point of view, the first *ab initio* study of $(CH_2O)_2$ was reported by Del Bene et *al.*[5] Subsequently, more sophisticated quantum chemical methodologies have been reported by Ford et *al.*[6] and recently by both Dolgonos[7] and Tschumper et *al.*[8] who predicted the existence of two different intermolecular potential energy minima with almost identical energies (Fig. 1). A predicted potential energy minimum of C_s symmetry involves one single weak intermolecular CH··O hydrogen bond motif leading to a perpendicular arrangement of oppositely oriented subunits. The second potential energy minimum of C_{2h} symmetry involves doubly weak intermolecular CH··O hydrogen bonds forming a complete planar arrangement of all atoms. The two recent high-level quantum chemical investigations independently conclude that the C_s configuration is the global potential energy minimum stabilized by 0.6–1.8 kJ·mol^{-1} relative to the local C_{2h} minimum.[7,8]

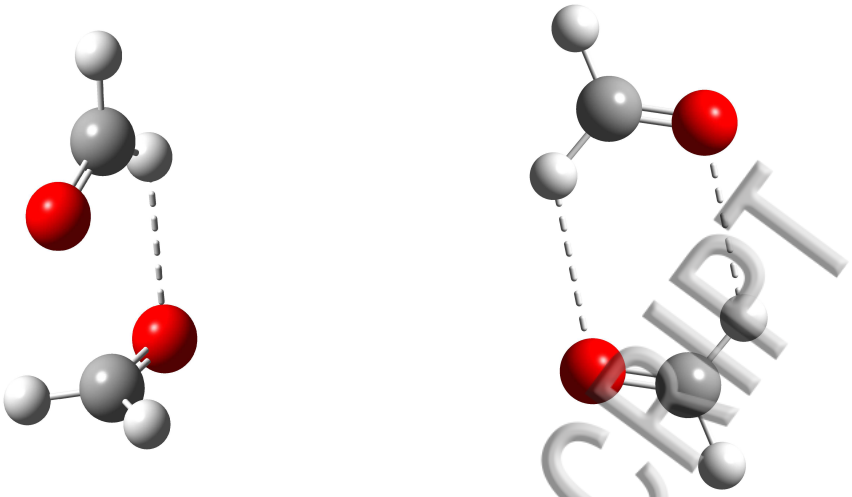

Figure 1: The two predicted intermolecular potential energy minima for $(CH_2O)_2$ involving double (C_{2h} symmetry, right) and single (C_s symmetry, left) weak intermolecular CH··O hydrogen bond motifs.

In several recent studies, we have shown experimentally how the interaction strength, directionality and anharmonicity of typical OH··O hydrogen bonds between molecules can be effectively probed *directly* in the far-infrared spectral region via the large-amplitude intermolecular vibrational motion introduced upon hydrogen bond formation.[9–14] In the present contribution, we demonstrate how the class of large-amplitude hydrogen bond librational modes in the THz region also provides *direct* excellent spectroscopic probes for the weak intermolecular CH··O hydrogen bond motifs of $(CH_2O)_2$ embedded in solid neon and para-hydrogen at 2.8 K.

2. Experimental

Isotopic gaseous samples of regular CH_2O (Sigma-Aldrich), CHDO (MSD Isotopes, 98% atom D) and CD_2O (Merck, 90% atom D) were prepared by cracking the respective *para*-formaldehyde polymers around 400 K in a vacuum line, passing the formed gaseous samples through a glass wool filter and a drying agent P_2O_5 before condensing the samples in a LN2 cold trap. Subsequently, the condensed samples were purified from CO and CO_2 by vacuum distillation around 200 K. For the preparation of doped neon matrices, approximately 0.02 mol of LN2 pre-cooled neon gas (Air Liquide, 99.999%) was deposited via a MKS multi range mass flow controller onto a gold-plated oxygen-free high thermal conductivity (OFHC) copper mirror at 3.6 K in a

specially designed immersion helium cryostat (IHC-3).[15,16] For the preparation of doped para-hydrogen matrices the same amount of LN2 pre-cooled para-hydrogen (>99.9%) was deposited manually from a 1000-mL Duran sample flask via a Swagelok low-flow metering valve. The highly enriched para-hydrogen samples were prepared from regular H_2 (Air Liquide, 99.999%) employing an ortho/para-hydrogen conversion dip-stick tube containing a paramagnetic hydrated iron(III)oxide catalyst (Sigma Aldrich, catalyst grade, 30–50 mesh). This conversion dip-stick was immersed in the cold gas over liquid helium iteratively above and below the triple point at 13.6 K for around 1.5 hour in a similar fashion as described by Andrews and co-workers.[17] The host gas was doped simultaneously with the regular or an isotopically substituted sample via separate inlet tubing systems resulting in mixing ratios in the order of (1:500–3000). A LakeShore temperature controller (Model 325) kept the mirror temperature at 2.8±0.1 K by the use of resistive heating and feedback electronics before and after the neon matrix deposition. Interchangeable CsI and polymethylpentene (TPX) windows were mounted on the vacuum shroud surrounding the cold head of the cryostat and IR and THz single-beam sample spectra were collected by a Bruker IFS 120 FTIR spectrometer via a specially designed optical arrangement guiding the focused probe beam onto the cold mirror in the cryostat. The IR single-beam spectra between 600 and 4500 cm^{-1} were all generated by a LN2 cooled HgCdTe detector combined with a Ge on KBr beam splitter and a globar radiation source. The corresponding THz single-beam spectra between 50 and 650 cm^{-1} were all generated by a LHe cooled Si-bolometer in combination with a 6 μm multilayer Mylar beam splitter and a globar radiation source. The single-beam background spectra of the evacuated cryostat were all subsequently collected. A spectral resolution in the range from 0.1 to 1.0 cm^{-1} was selected depending on the observed band widths. In all experiments the doped matrices were annealed up to 9 K (neon) and 4.2 K (para-H_2) to reveal potential temperature effects.

3. Vibrational Assignments of Formaldehyde Dimer in Solid Neon Matrices

Fig. 2 shows a series of THz absorption spectra in the range between 75 and 200 cm^{-1} collected for cryogenic neon matrices doped with regular CH_2O and isotopically enriched CD_2O and CDHO samples at 2.8 K with (1:1300) mixing ratios. A number of dominant spectral features are reproduced at 84 cm^{-1} and close to the experimental cut-off at 63 cm^{-1} (not shown) for all the neon matrices doped with regular CH_2O. The two bands are even observed at very low CH_2O concentrations and always decrease in intensity upon annealing and therefore assigned to rotational-translation-coupling (RTC) transitions of CH_2O monomers embedded in the cages of the solid neon host. Similar strong monomeric RTC transitions have been reported for H_2O[18] and CH_3OH embedded in solid neon cages.[19] In doped neon matrices with higher CH_2O concentrations, two new distinct bands clearly appear in the spectra around 167 and 123 cm^{-1} with a relative intensity around 1:5 and the latter apparently somewhat broader than the former. Both observed bands have a steeper concentration dependency than the assigned monomeric RTC bands pointing at potential vibrational assignments to $(CH_2O)_2$. The annealing of doped neon matrices up to 10 K has previously proven a valuable tool to verify complex formation as

the "warm" and soft neon matrices allow the diffusion of small sample molecules and promote the further build-up of molecular complexes in the matrix.[11,13,14,16] The post-annealing THz spectrum shown in Fig. 2 reveal that both bands observed at 167 and 123 cm^{-1} gain intensity after the annealing procedures and strongly supports the proposed $(CH_2O)_2$ origin of both bands. The post-annealing spectra tentatively reveal a third band around 95 cm^{-1}, which is hard to assign unambiguously owing to the stronger RTC band in the neon matrices. However, at this stage the assignment of the three bands is still not clear and it would be informative to learn whether the observed build-up of molecular complexes could be caused by small amounts of highly mobile H_2O molecules in the "hot" matrix forming mixed complexes of CH_2O and H_2O.

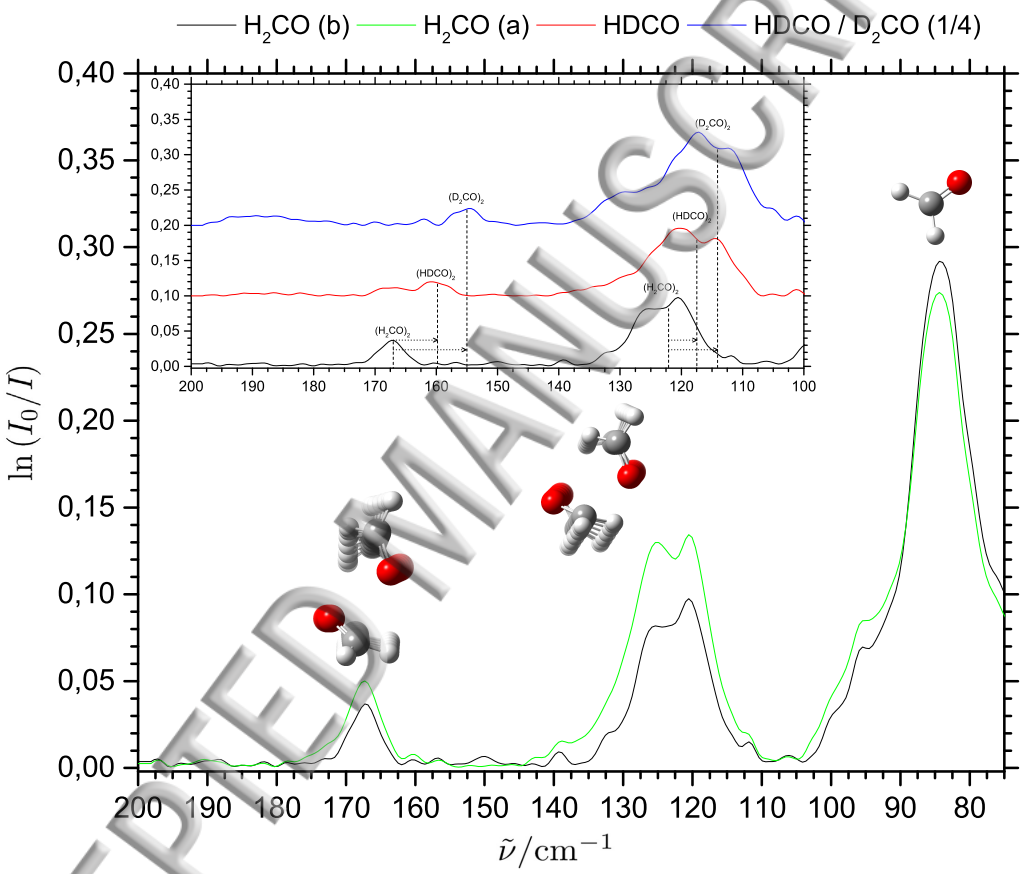

Figure 2: THz absorption spectra in the 75–200 cm^{-1} region recorded for neon matrices doped with CH_2O, CHDO and CD_2O (mixing ratio of 1:1300) at 2.8 K before (black curve) and after (green curve) annealing to 10 K with proposed vibrational assignments of the acceptor *b*-axis and donor *c*-axis librational bands of $(CH_2O)_2$. The inset shows the observed isotopic spectral shifts for $(CHDO)_2$ (red curve) and $(CD_2O)_2$ (blue curve).

In order to rule out the formation of mixed CH_2O–H_2O complexes, a series of complementary neon matrix experiments doped simultaneously with CH_2O and H_2O have been carried out (not shown). The THz absorption of both H_2O monomer and $(H_2O)_2$ embedded in cryogenic neon matrices have been studied extensively by Ceponkus and Nelander in a series of works.[15,20–22] The overall rotational motion of H_2O monomer is just slightly hindered in neon matrices and

the two strong rotational transitions at 33 ($1_{11}\leftarrow 0_{00}$) and 52 cm^{-1} ($2_{12}\leftarrow 1_{01}$) have been assigned in neon matrices at 2.8 K besides the two strong monomeric RTC transitions. The two most infrared active large-amplitude intermolecular fundamental vibrational transitions of $(H_2O)_2$ in the THz region, the donor torsional mode and the acceptor wagging mode (a-axis libration), have previously been observed and assigned at 116.0 cm^{-1} and 122.2 cm^{-1}, whereas the less infrared active acceptor twist (c-axis libration) fundamental transition has been assigned at 150.6 cm^{-1} in the neon matrix environment. None of these bands except traces of the extremely intense pure rotational transitions at 32 and 52 cm^{-1} appear in the present neon matrices doped with CH_2O alone. The THz spectra obtained for the neon matrices doped with CH_2O/H_2O mixtures revealed three additional bands in the combined far-IR and THz region below 500 cm^{-1}, which shall not be described in more detail in the present contribution. However, we mention here that one of the bands for the mixed CH_2O–H_2O complex is reproduced at 168 cm^{-1} and thereby slightly but significantly shifted relative to the band observed at 167 cm^{-1} in the matrices doped solely with CH_2O.

The inset of Fig. 2 shows the THz spectra obtained for neon matrices doped with regular CH_2O and isotopically enriched samples of CHDO and CD_2O. It is evident that the isotopic H/D substitutions result in significant spectral red-shifts for the bands observed for regular CH_2O at 167 and 123 cm^{-1}. The mono-deuteration of CH_2O is clearly red-shifting the most intense 123 cm^{-1} band by 5 cm^{-1}, whereas the di-deuteration of CH_2O clearly produces a red-shift of 8 cm^{-1}. The isotopic spectral shifts for the much less intense band observed for regular CH_2O at 167 cm^{-1} are more difficult to extract close to the detection limit but reproducible spectral red-shifts of 8 and 12 cm^{-1} are confidently monitored upon mono- and di-deuteration, respectively. It should be mentioned here that the significant CHDO content of the CD_2O sample affects the band shapes in the THz spectra collected for CD_2O. In particular, the stronger but also significantly broader band around 115 cm^{-1} in the CD_2O spectrum becomes slightly asymmetric due to the isotopic overlap. A similar asymmetry is observed for the CDHO band at 118 cm^{-1} due to isotopic overlap with the regular CH_2O band at 123 cm^{-1}. In order to reproduce these experimental findings and confirm the existence of monomeric RTC transitions of CH_2O in the neon cages, similar matrix isolation experiments have been done employing highly enriched para-H_2 hosts with significantly larger cage sizes (39 Å^3) than for solid neon (22 Å^3). A previous investigation by Nelander et *al.*[23] has shown that enriched para-H_2 matrices doped with H_2O do not give rise to strong and broad RTC bands in the THz region.

4. Vibrational Assignments of Formaldehyde Dimer in Solid Para-Hydrogen Matrices

In order to estimate the ortho/para-H_2 conversion efficiency, the relative integrated intensities of the sharp ro-vibrational $Q_1(0)$ and $S_1(0)$ lines observed at 4152.9 cm^{-1} and 4485.9 cm^{-1} shown in Fig. 3, which become infrared active due to perturbations in the solid matrix, have been determined for a series of thinner (ca. 0.01 mol) para-H_2 matrices without dopants. This $S_1(0)/Q_1(0)$ intensity ratio provides an estimate of the para-H_2 enrichment[17,24] and the present

This manuscript was accepted by J. Chem. Phys. Click here to see the version of record.

average value above 50 indicates enrichments better than 99.9% para-H_2.

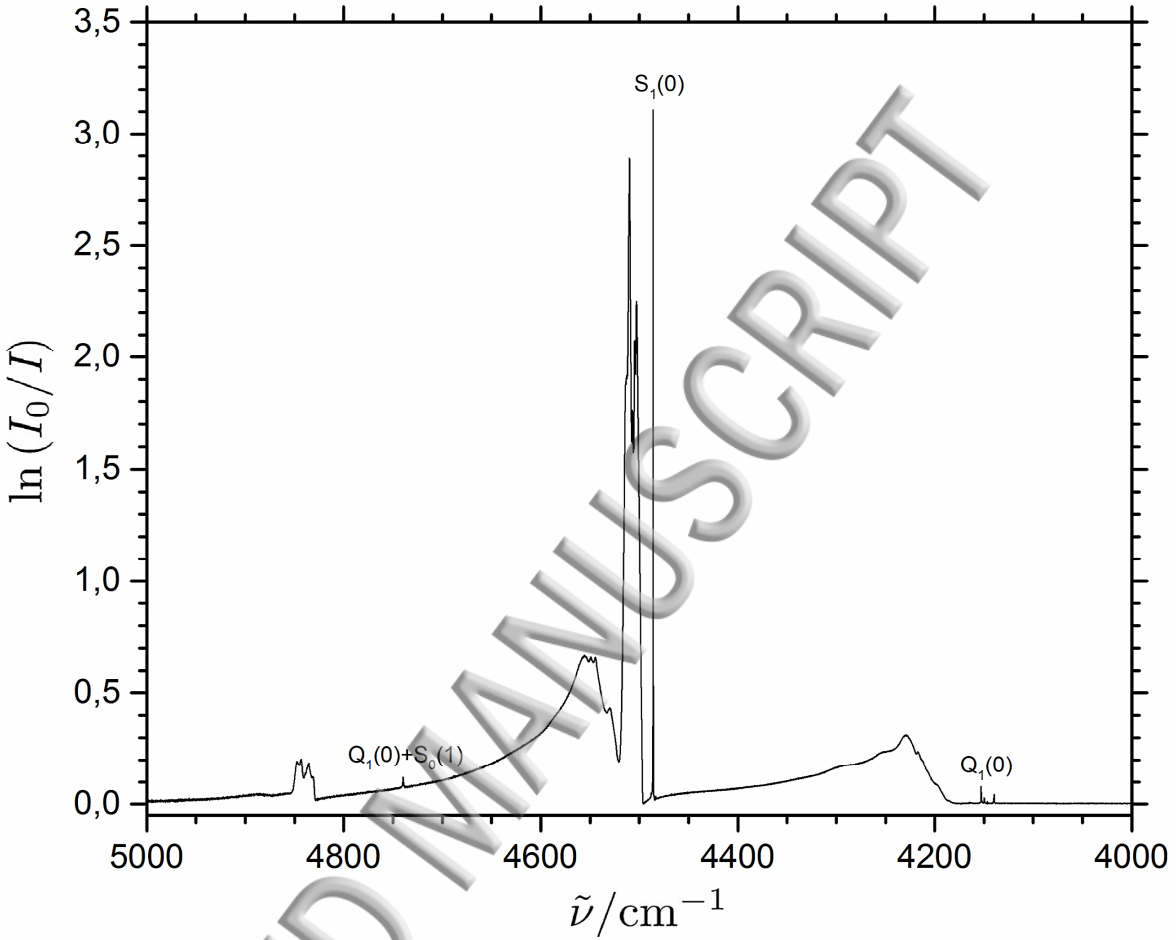

Figure 3: The mid-IR absorption spectrum (4000–5000 cm^{-1}, 0.1 cm^{-1} resolution) for a non-doped para-H_2 matrix (≈0.01 mol, 99.9% enriched) with assignments of the ro-vibrational $Q_1(0)$ and $S_1(0)$ lines.

Fig. 4 shows a series of THz absorption spectra in the range between 60 and 200 cm^{-1} collected both for a pure enriched para-H_2 matrix and several enriched para-H_2 matrices doped with regular CH_2O and isotopically enriched CD_2O and CDHO samples at 2.8 K with mixing ratios in the order of (CH_2O:para-H_2)=(1:500–900). The absorption spectra all reproduce the pure rotational $S_0(0)$ transition observed previously by Nelander et *al.*[23] consisting of a very narrow zero phonon line at 355.6 cm^{-1} accompanied by a very broad phonon wing extending up to approximately 600 cm^{-1} (not shown). The THz spectrum of the pure para-H_2 matrix demonstrates that the solid para-H_2 medium provides an excellent spectroscopic THz window below 355.6 cm^{-1} which is highly suitable for matrix isolation. Besides the strong narrow zero phonon line, two distinct bands are clearly observed at 153 and 110 cm^{-1} as soon as the matrices are doped with CH_2O, the latter band with an extra low-wavenumber shoulder around 83 cm^{-1}. The observed spectral features are broader than the similar bands observed in the

doped neon matrices and explain why slightly higher mixing ratios have been employed. The third band positions are shifted by nearly 10% relative to the three bands observed at 167, 123 and ~95 cm^{-1} in the neon matrices but the band intensity ratio of the two distinct bands at higher wavenumbers is almost identical. In addition, the intensities of the two observed bands increase similarly with higher concentration although a quantitative measure of this concentration dependence is challenging due to the overlap with the third band at 83 cm^{-1}. Nevertheless, the observed concentration dependence pattern suggests the existence of three distinct bands belonging to the same molecular cluster without any disturbing RTC transitions.

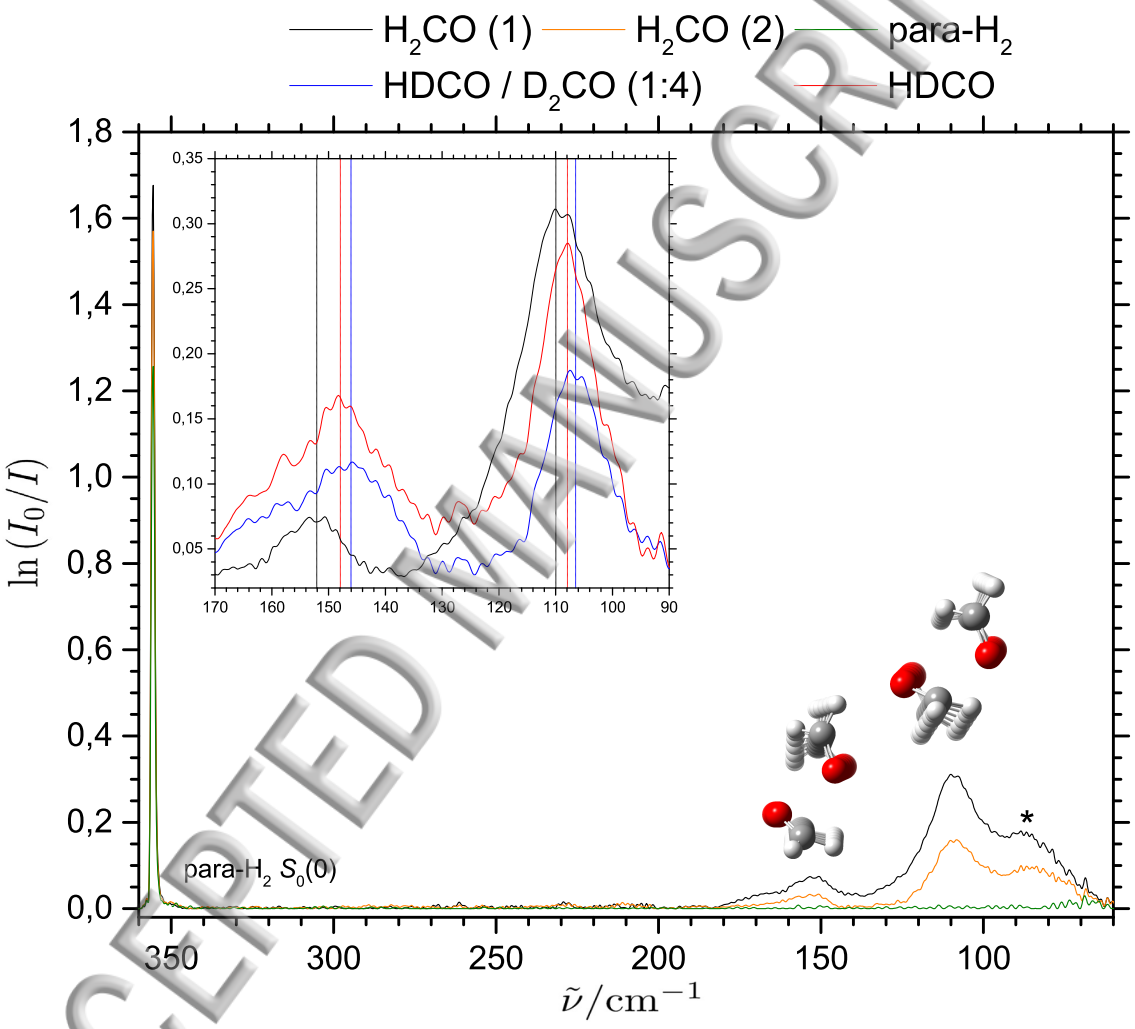

Figure 4: THz absorption spectra in the 60–370 cm^{-1} region recorded for a pure enriched para-H_2 (99.9% enriched) matrix (green curve) and two para-H_2 matrices doped with CH_2O at two different mixing ratios (orange and black curves) at 2.8 K with proposed vibrational assignments of the acceptor *b*-axis and donor *c*-axis librational bands of $(CH_2O)_2$. The inset shows the observed isotopic spectral shifts for $(CHDO)_2$ (red curve) and $(CD_2O)_2$ (blue curve). The asterisk indicates the tentative assignment of the donor *b*-axis librational band.

The isotopic H/D substitutions result in significant spectral red-shifts for the observed bands although these are slightly smaller than observed in the THz spectra of the doped neon matrices.

This manuscript was accepted by J. Chem. Phys. Click here to see the version of record.

The inset of Fig. 4 shows the THz spectra obtained for para-H_2 matrices doped with regular CH_2O and isotopically enriched samples of CHDO and CD_2O. The mono-deuteration of CH_2O is red-shifting the less intense 154 cm^{-1} band by 4.5 cm^{-1}, whereas the di-deuteration of CH_2O produces a larger red-shift of 7 cm^{-1}. Somewhat smaller spectral red-shifts are monitored upon mono- and di-deuteration, respectively, for the stronger band observed for regular CH_2O at 110 cm^{-1}, although the exact values are hard to extract accurately due to the larger band widths in the para-H_2 matrices and the limited purity of the CD_2O sample. The significant content of CHDO in the CD_2O sample results in severely overlapped bands for the para-H_2 matrices doped with CHDO and CD_2O. The isotopic spectral shifts of the third band around 83 cm^{-1} on the shoulder of the 110 cm^{-1} band cannot be verified due to the extra spectral noise in this spectral region close to the experimental cut-off. However, the existence of this extra third band is reproduced in all the THz spectra recorded. These observations are thus consistent with the appearance of the third spectral feature on the shoulder of the strong RTC band after the annealing of the neon matrices. At this point in the spectral analysis, it would be highly desirable to learn more from quantum chemical predictions, which are amenable for a molecular system of this limited size.

5. Exploratory Quantum Chemical Calculations

The software packages Gaussian09 (Rev. D.01)[25] and MOLPRO (ver. 2012.1)[26,27] have been employed for high-level electronic structure calculations. The potential energy minima geometries of the CH_2O monomer and two different potential energy minima of $(CH_2O)_2$ of C_s and C_{2h} symmetry have all been optimized using the second-order Möller-Plesset MP2 method[28,29] in combination with Dunning's augmented correlation-consistent quadruple-zeta (aug-cc-pVQZ) basis set.[30] The RMS force criterion has been set to 10^{-6} (atomic units) for these optimizations and the harmonic vibrational band origins have been computed at the optimized structures. The single-point electronic energies for the optimized minima structures have subsequently been computed employing the coupled-cluster approach with single and double excitations and perturbative treatment of triple excitations CCSD(T)[31] and also the explicitly-correlated CCSD(T)-F12b methodology,[32] as implemented in the MOLPRO package, combined with employing Dunning's series of correlation-consistent aug-cc-pV(T,Q,5)Z basis sets to optimize the treatment of electron correlation effects. The basis set superposition errors[33] have been accounted for by the implemented counterpoise methods.[34]

The computed the electronic complexation energies D_e from the MP2, CCSD(T) and CCSD(T)-F12b methods with Dunning's correlation-consistent and augmented aug-cc-pV(T,Q,5)Z basis sets are provided in Table 1. Table 2 provides the predicted harmonic frequencies and corresponding harmonic band intensities together with predicted isotopic spectral shifts at the MP2/aug-cc-pVQZ level for the classes of six large-amplitude intermolecular vibrational modes for the two different potential energy minima of C_s and C_{2h} symmetry.

Table 1: The electronic dissociation energies D_e (kJ/mol) for two potential energy minima of C_s and C_{2h} symmetry for $(CH_2O)_2$ at the MP2, CCSD(T) and CCSD(T)-F12b levels employing Dunning's correlation-consistent aug-cc-pV(T,Q,5)Z basis sets based on at the counterpoise (CP)-corrected MP2/aug-cc-pVQZ level.

Electronic Energy Method	$(H_2CO)_2$ C_{2h}	$(H_2CO)_2$ C_s
MP2/aug-cc-pVQZ	15.18	19.55
MP2-CP/aug-cc-pVQZ	14.41	18.66
CCSD(T)/aug-cc-pVTZ	16.41	19.60
CCSD(T)-F12b/aug-cc-pVTZ	16.24	19.59
CCSD(T)/aug-cc-pVQZ	16.10	19.39
CCSD(T)-F12b/aug-cc-pVQZ	15.99	19.29
CCSD(T)/aug-cc-pV5Z	15.92	19.17
CCSD(T)-F12b/aug-cc-pV5Z	15.91	19.17

6. Results and Discussions

The first interesting result from the quantum chemical predictions, in terms of the assignment procedure, concerns the actual number of infrared active large-amplitude intermolecular vibrational modes for the two potential energy minima of $(CH_2O)_2$ in the THz spectral region considered for the present experimental work. The harmonic MP2/aug-cc-pVQZ calculations for the C_{2h} potential energy minimum reveal only one single infrared active intermolecular mode above 75 cm^{-1}, whereas the calculations for the C_s conformation forecast three different infrared active intermolecular modes. Both the predicted harmonic band origins and corresponding relative intensities for the C_s conformation agree well with the present spectroscopic observations, although the double harmonic approximation may be inaccurate for such a weakly bound molecular system. The predicted relative harmonic band strengths of 1:5:3 for the three infrared active modes of the C_s conformation are in close agreement with the relative integrated band intensities of the three bands observed at 151, 110 and 83 cm^{-1} in the doped para-H_2 matrices. The predicted relative harmonic band strength of 1:5 also fits the relative integrated intensity of the two bands observed at 167 and 123 cm^{-1} in the doped neon matrices. A closer look at the harmonic normal mode predictions reveal that the three infrared active large-amplitude vibrational modes all involve hindered overall rotational motion around the principal b-axis or c-axis of the CH_2O subunits as animated in Fig. 5. The infrared active vibrational mode with the smallest predicted band intensity of 9 km·mol^{-1} can be depicted as a c-axis librational mode of the hydrogen bond donor subunit in the symmetry plane spanned by the two intermolecular CH··O and C··O contacts around the principal c-axis of the isolated subunit as shown in Fig. 5 (right). The vibrational mode with the largest predicted band intensity of 52 km·mol^{-1}, on the other hand, can be depicted as a b-axis librational mode (acceptor wagging mode) of the hydrogen bond acceptor subunit as shown in Fig. 5 (left), whereas the third vibrational mode with medium infrared activity of 31 km·mol^{-1} can be depicted as a similar b-axis libration (donor wagging mode) of the hydrogen bond donor (not shown). The three

remaining more or less infrared forbidden intermolecular vibrational modes can be depicted as one intermolecular stretching mode and two a-axis librational modes of the acceptor and donor subunits. The latter two torsional degrees of freedom both describing the hindered rotational motion around the C=O bonds of the subunits therefore do not give rise to any dipole moment changes.

Table 2: The predicted harmonic frequencies (cm^{-1}) and corresponding harmonic band intensities ($km \cdot mol^{-1}$) of the class of six large-amplitude intermolecular vibrational modes for the three isotopic variants $(CH_2O)_2$, $(CHDO)_2$ and $(CD_2O)_2$ at the MP2/aug-cc-pVQZ level.

	$(CH_2O)_2$		$(CHDO)_2$		$(CD_2O)_2$	
Mode	C_{2h}	C_s	C_{2h}	C_s	C_{2h}	C_s
1	62.0 (31)	89.6 (31)	61.3 (32)	83.0 (27)	53.6 (15.9)	79.5 (24)
2	65.1 (0.0)	115.6 (0.1)	63.2 (0.0)	114.4 (0.1	62.3 (0.0)	113.2 (0.2)
3	88.4 (4.2)	156.7 (52)	71.2 (0.1)	146.8 (41)	66.1 (13.5)	137.8 (0.0)
4	93.9 (0.0)	194.1 (0.0)	78.1 (0.0)	164.4 (6.3)	67.1 (0.2)	141.8 (32)
5	123.1 (0.0)	208.0 (8.8)	115.9 (0.0)	193.8 (7.6)	111.7 (0.0)	186.1 (6.0)
6	139.2 (58.7)	289.4 (0.4)	129.9 (51)	246.5 (2.5)	122.4 (45)	209.1 (0.8)

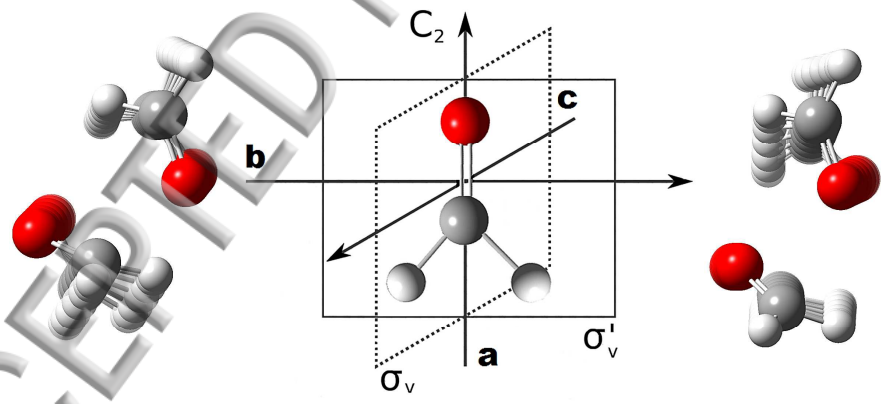

Figure 5: The animated large-amplitude hydrogen bond vibrational modes of the global potential energy minimum of $(CH_2O)_2$ together with the principal coordinate system for a CH_2O subunit (center). The two observed low-frequency mode resembles an acceptor b-axis librational mode (left) whereas the observed high-frequency mode resembles a donor c-axis librational mode (right).

This manuscript was accepted by J. Chem. Phys. Click here to see the version of record.

Despite the severe limitations of the harmonic approximation for this class of intermolecular vibrational motion, the harmonic predictions qualitatively support the experimental isotopic spectral shifts associated with the H/D substitutions of CH_2O. The harmonic isotopic spectral red-shifts predicted for the complete deuteration of the CH_2O monomer are approximate 50% larger than the predicted isotopic spectral shifts for the mono-deuteration of CH_2O for all three infrared active large-amplitude libational modes of the C_s conformation of $(CH_2O)_2$. This pattern is in excellent agreement with the spectroscopic findings for the acceptor b-axis and donor c-axis librational bands, whereas the predicted isotopic spectral shifts for the low-wavenumber donor b-axis librational band origin cannot be compared to experimental values in the present work. In the harmonic approximation, the librational band origins are furthermore directly proportional to the square root of the corresponding rotational constants for the isolated subunits. The inspection of known values for the rotational constants B_0 and C_0 of the isolated subunits CH_2O, CHDO and CD_2O[35] reveals that this simple harmonic model indeed qualitatively predicts the correct order of the observed isotopic spectral shifts both for the assigned donor c-axis libration and the acceptor b-axis libration. The c-axis librational band origins are slightly more affected by H/D substitutions than the b-axis librational band origins in accordance with the observed isotopic shifts both in the neon and para-H_2 matrices and further support the proposed assignments.

The large-amplitude nature of the intermolecular vibrational motion for $(CH_2O)_2$ is expected to involve substantial anharmonic contributions to the band origins in the order of 15–25% due to the very shallow potential energy surface describing the weak intermolecular CH··O hydrogen bond motif.[13,14,16,36,37] The direct comparison between the experimental observations and the harmonic MP2/aug-cc-pVQZ predictions indeed indicates deviations in the order of 20% (neon matrices) to 30% (para-H_2 matrices). These observed deviations can thus probably to a large extent be ascribed to the mechanical anharmonicity of the large-amplitude intermolecular vibrational coordinates, although additional smaller spectral shifts associated with perturbations induced by the cages in the matrix hosts may be included. The smaller matrix cages in neon relative to para-H_2 may explain the higher band origins observed in neon matrices as minor repulsive steric effects may originate from the more congested neon host environment. However, both a recent far-infrared vibration-rotation-tunneling (VRT) study of $(H_2O)_2$ probed in molecular beams[38] and recent far-infrared jet studies of alcohol dimers have revealed minor neon matrix spectral blue-shifts relative to gas phase in the sub-% range for large-amplitude out-of-plane intermolecular donor OH librational band origins of these prototypical hydrogen-bonded cluster molecules.[11,39] Based on these independent investigations, the present neon matrix isolation findings are considered to have near-gas-phase quality in the investigated THz region. The combined experimental findings thus provide overwhelming experimental evidence for the existence of the C_s potential energy minima of $(CH_2O)_2$ in the cryogenic neon and para-H_2 environment. The scaled harmonic predictions suggest that two infrared active bands associated with large-amplitude vibrational motion of the C_{2h} conformation would be observable around 110 and 50 cm^{-1} in the neon matrices. However, the latter transition energy is outside the present experimental cut-off and the THz spectra for the doped neon matrices do

This manuscript was accepted by J. Chem. Phys. Click here to see the version of record.

not reveal any distinct band around 110 cm^{-1}.

Table 3: The electronic dissociation energy D_e, the total change of harmonic vibrational zero-point energy upon complexation ΔZPE and the resulting absolute dissociation energy D_0 for the two most stable C_s and C_{2h} conformations of $(CH_2O)_2$ (units of kJ·mol^{-1}).

	Model	CCSD(T)-F12/aug-cc-pVTZ[a] Tschumper et *al.*[8]	CCSD(T)/CBS[b] Dolgonos[7]	CCSD(T)-F12b/aug-cc-pV5Z[c] Present work
C_s	D_e	19.2	18.5	19.2
	ΔZPE	6.9	5.4	5.5
	D_0	12.3	13.1	13.7
C_{2h}	D_e	15.8	15.0	
	ΔZPE	4.1	3.7	
	D_0	11.7	11.3	

[a] Electronic energies for optimized geometries at the MP2/aug-cc-pVTZ level. The ΔZPE-value is based on harmonic force fields at the MP2/aug-cc-pVTZ level.

[b] The ΔZPE-value is based on anharmonic (VPT2) force fields at the MP2/aug-cc-pVTZ level.

[c] Electronic energies for counterpoise-corrected geometries at the MP2/aug-cc-pVQZ level. The ΔZPE-value is based on semi-empirical force fields (see text).

The observation of three large-amplitude vibrational transitions enables the first reliable determination of a semi-empirical value for the change of vibrational zero-point energy upon complexation (ΔZPE) of the two CH_2O subunits. An accurate theoretical value for this quantity, including the anharmonic contributions from the class of large-amplitude hydrogen bond vibrational motion, is notoriously difficult to predict. In a recent work Dolgonos[7] reported an anharmonic treatment at the MP2/aug-cc-pVTZ level based on second-order vibrational perturbation theory[40–44] in its implementation by Barone (VPT2)[40,45] in conjunction with harmonic frequencies at the CCSD(T)/aug-cc-pVQZ level (Table 3). These anharmonic vibrational zero-point energy corrections translated the dissociation energy at equilibrium for the potential energy minimum C_s of 18.5 kJ·mol^{-1} computed in the CCSD(T)/CBS limit into a D_0-value of 13.1 kJ·mol^{-1}. In a similar approach a D_0-value of 11.3 kJ·mol^{-1} was obtained in the CCSD(T)/CBS limit for the local C_{2h} potential energy minimum (Table 3). The large-amplitude vibrational motion for the shallow potential energy surface of $(CH_2O)_2$, however, probably challenges the applicability of this VPT2 approximation and we propose here an experimentally rooted value of ΔZPE based on the present THz observations. The fact that our harmonic MP2/aug-cc-pVQZ predictions overshoot the two unambiguously assigned hydrogen bond librational band origins from the neon matrix with 20% suggests a uniform scaling factor of this size for the complete class of six large-amplitude intermolecular vibrational modes. This simple scaling approach, which corrects the harmonic predictions for the unavailable contributions from mechanical anharmonicity and potential matrix shifts for the three remaining modes, should ideally treat these three modes individually as both the anharmonicity constants and the matrix cage perturbations obviously depend on the specific vibrational coordinates. How-

This manuscript was accepted by J. Chem. Phys. Click here to see the version of record.

ever, these individual scaling factors for the three remaining infrared forbidden large-amplitude modes are not accessible at this point. The uniform scaling approach for the remaining three intermolecular modes provides a semi-empirical value of 5.0 kJ·mol^{-1} for the intermolecular part of ΔZPE upon complexation. The anharmonic contributions to the minor complexation shifts of the small-amplitude intramolecular vibrational modes of $(CH_2O)_2$ can be neglected as the total harmonic value for the intramolecular part of ΔZPE is 0.5 kJ·mol^{-1} (see the Supplemental Material). The resulting total semi-empirical ΔZPE-value of 5.5 kJ·mol^{-1} is estimated to have an error of ±0.3 kJ·mol^{-1} owing to potential non-uniform anharmonicity corrections and non-uniform minor perturbations by the neon matrix host. This semi-empirical ΔZPE-value interestingly agrees perfectly well with Dolgonos' prediction based on second-order vibrational perturbation theory.[7] The present electronic energies at the CCSD(T)-F12b/aug-cc-p5Z level, based on counterpoise-corrected MP2/aug-cc-pVQZ optimized geometries, provides a D_e-value of 19.2 kJ·mol^{-1} as shown in Table 2. This result is in excellent agreement with the recent work by Tschumper et *al.*[8] and a resulting semi-empirical estimate for the dissociation energy D_0 of 13.7±0.3 kJ·mol^{-1} is then obtained for the global potential energy minimum of $(CH_2O)_2$ (Table 3).

6. Conclusions

To conclude, the present THz observations of CH_2O embedded in neon and para-H_2 matrices based on combined concentration dependency measurements, dedicated annealing experiments and the use of isotopically enriched CH_2O samples allow for the unambiguous assignment of three of the six large-amplitude intermolecular vibrational modes for $(CH_2O)_2$. In the neon matrices, the two infrared active vibrational bands associated with the donor *c*-axis librational mode and the acceptor *b*-axis librational mode (acceptor wagging mode) are observed at 167 and 123 cm^{-1}, respectively, whereas the third band around 95 cm^{-1} associated with the donor *b*-axis librational mode (donor wagging mode) is severely overlapped by a strong rotational-translation-coupling transition of CH_2O induced by the tight neon matrix cages. In a series of complementary THz investigations of $(CH_2O)_2$ embedded in 99.9% para-H_2 matrices with significantly larger matrix cages, all three large-amplitude intermolecular vibrational bands are observed at 151, 110 and 83 cm^{-1} owing to the lack of rotational-translation-coupling bands and thereby all shifted by approximately 10% relative to the neon observations. The combined spectroscopic observables are in excellent agreement with the present and recent high-level quantum chemical calculations suggesting that the C_s conformation of $(CH_2O)_2$ is the global potential energy minimum.[7,8] The present experimental THz observations enable the first reliable semi-empirical determination of the change of vibrational zero-point energy (ΔZPE) of 5.5 ±0.3 kJ·mol^{-1} for the $(CH_2O)_2$ complexation process. This semi-empirical value interestingly agrees perfectly well with Dolgonos' recent prediction based solely on second-order vibrational perturbation theory.[7] The combination with an electronic dissociation energy D_e of 19.2 kJ·mol^{-1} computed at the CCSD(T)-F12b/aug-cc-p5Z level based on counterpoise-corrected MP2/aug-cc-pVQZ optimized geometries, then provides a D_0-value of 13.7±0.3 kJ·mol^{-1} for the global C_s potential energy minimum of $(CH_2O)_2$.

Supplemental Material

The calculated absolute electronic energies employing the MP2, CCSD(T) and CCSD(T)-F12 methodologies with Dunning's correlation-consistent the aug-cc-pV(V,Q,5)Z basis sets and the calculated harmonic vibrational zero-point energy corrections employing the MP2/aug-cc-pVQZ method are given as supplementary material.

Acknowledgements

The authors appreciate interesting discussions with B. Nelander and A. Engdahl. The authors acknowledge DTU Computing Center for access to the High Performance Computing services. RWL acknowledges financial support from the Danish Council for Independent Research's Sapere Aude Programme (Grant Ref.: 12-125248).

References

[1] Steiner, T. *Angewandte Chemie International Edition* **2002**, *41*(1), 48–76.

[2] Khoshkhoo, H.; Nixon, E. R. *Spectrochimica Acta Part A: Molecular Spectroscopy* **1973**, *29*(4), 603–612.

[3] Nelander, B. *The Journal of Chemical Physics* **1980**, *73*(3), 1026.

[4] Lovas, F. J.; Suenram, R. D.; Coudert, L. H.; Blake, T. A.; Grant, K.; Novick, S. E. *The Journal of Chemical Physics* **1990**, *92*(2), 891.

[5] Del Bene, J. E. *The Journal of Chemical Physics* **1974**, *60*(10), 3812.

[6] Ford, T.; Glasser, L. *Journal of Molecular Structure: THEOCHEM* **1997**, *398-399*, 381–394.

[7] Dolgonos, G. A. *Chemical Physics Letters* **2013**, *585*, 37–41.

[8] Van Dornshuld, E.; Holy, C. M.; Tschumper, G. S. *Journal of Physical Chemistry A* **2014**, *118*(18), 3376–3385.

[9] Wugt Larsen, R.; Suhm, M. A. *The Journal of Chemical Physics* **2006**, *125*(15), 154314–154314.

[10] Wugt Larsen, R.; Suhm, M. *Physical Chemistry Chemical Physics* **2010**, *12*(29), 8152–8157.

[11] Kollipost, F.; Andersen, J.; Mahler, D. W.; Heimdal, J.; Heger, M.; Suhm, M. A.; Wugt Larsen, R. *Journal of Chemical Physics* **2014**, *141*(17), 174314.

[12] Kollipost, F.; Wugt Larsen, R.; Domanskaya, A. V.; Noerenberg, M.; Suhm, M. A. *The Journal of Chemical Physics* **2012**, *136*(15).

[13] Andersen, J.; Heimdal, J.; Wugt Larsen, R. *Phys. Chem. Chem. Phys* **2015**, *17*(37), 23761–23769.

[14] Andersen, J.; Heimdal, J.; Wugt Larsen, R. *Journal of Chemical Physics* **2015**, *143*(22), 224315.

[15] Ceponkus, J.; Uvdal, P.; Nelander, B. *The Journal of Chemical Physics* **2008**, *129*(19), 194306.

[16] Andersen, J.; Heimdal, J.; Mahler, D. W.; Nelander, B.; Wugt Larsen, R. *Journal of Chemical Physics* **2014**, *140*(9), 091103.

[17] Andrews, L.; Wang, X. *Review of Scientific Instruments* **2004**, *75*, 3039–3044.

[18] Ceponkus, J.; Uvdal, P.; Nelander, B. *The Journal of Chemical Physics* **2013**, *138*(24), 244305.

[19] Perchard, J. *Chemical Physics* **2007**, *332*(1), 86–94.

[20] Ceponkus, J.; Nelander, B. *The Journal of Physical Chemistry A* **2004**, *108*(31), 6499–6502.

[21] Ceponkus, J.; Uvdal, P.; Nelander, B. *The Journal of Chemical Physics* **2010**, *133*(7), 074301.

[22] Ceponkus, J.; Uvdal, P.; Nelander, B. *The Journal of Physical Chemistry A* **2010**, *114*(25), 6829–6831.

[23] Ceponkus, J.; Uvdal, P.; Nelander, B. *The Journal of Physical Chemistry A* **2008**, *112*, 3921–3926.

[24] Tam, S.; Fajardo, M. E. *Review of Scientific Instruments* **1999**, *70*, 1926–1932.

[25] Gaussian09 Revision D.01. Frisch, M. J.; Trucks, G. W.; Schlegel, H. B.; Scuseria, G. E.; Robb, M. A.; Cheeseman, J. R.; Scalmani, G.; Barone, V.; Mennucci, B.; Petersson, G. A.; Nakatsuji, H.; Caricato, M.; Li, X.; Hratchian, H. P.; Izmaylov, A. F.; Bloino, J.; Zheng, G.; Sonnenberg, J. L.; Hada, M.; Ehara, M.; Toyota, K.; Fukuda, R.; Hasegawa, J.; Ishida, M.; Nakajima, T.; Honda, Y.; Kitao, O.; Nakai, H.; Vreven, T.; Montgomery, Jr., J. A.; Peralta, J. E.; Ogliaro, F.; Bearpark, M.; Heyd, J. J.; Brothers, E.; Kudin, K. N.; Staroverov, V. N.; Kobayashi, R.; Normand, J.; Raghavachari, K.; Rendell, A.; Burant, J. C.; Iyengar, S. S.; Tomasi, J.; Cossi, M.; Rega, N.; Millam, J. M.; Klene, M.; Knox, J. E.; Cross, J. B.; Bakken, V.; Adamo, C.; Jaramillo, J.; Gomperts, R.; Stratmann, R. E.; Yazyev, O.; Austin, A. J.; Cammi, R.; Pomelli, C.; Ochterski, J. W.; Martin, R. L.; Morokuma, K.; Zakrzewski, V. G.; Voth, G. A.; Salvador, P.; Dannenberg, J. J.; Dapprich, S.; Daniels, A. D.; Farkas, .; Foresman, J. B.; Ortiz, J. V.; Cioslowski, J.; Fox, D. J. **2009**.

[26] Werner, H.-J.; Knowles, P. J.; Knizia, G.; Manby, F. R.; Schtz, M. *WIREs Comput. Mol. Sc.* **2012**, *2*, 242–253.

[27] Molpro, version 2015.1, a package of ab initio programs. Werner, H.-J.; Knowles, P. J.; Knizia, G.; Manby, F. R.; Schütz, M.; Celani, P.; Györffy, W.; Kats, D.; Korona, T.; Lindh, R.; Mitrushenkov, A.; Rauhut, G.; Shamasundar, K. R.; Adler, T. B.; Amos, R. D.; Bernhardsson, A.; Berning, A.; Cooper, D. L.; Deegan, M. J. O.; Dobbyn, A. J.; Eckert, F.; Goll, E.; Hampel, C.; Hesselmann, A.; Hetzer, G.; Hrenar, T.; Jansen, G.; Köppl, C.; Liu, Y.; Lloyd, A. W.; Mata, R. A.; May, A. J.; McNicholas, S. J.; Meyer, W.; Mura, M. E.; Nicklass, A.; O'Neill, D. P.; Palmieri, P.; Peng, D.; Pflüger, K.; Pitzer, R.; Reiher, M.; Shiozaki, T.; Stoll, H.; Stone, A. J.; Tarroni, R.; Thorsteinsson, T.; Wang, M. **2015**.

[28] Møller, C.; Plesset, M. S. *Physical Review* **1934**, *46*, 618–622.

[29] Krishnan, R.; Pople, J. A. *International Journal of Quantum Chemistry* **1978**, *14*(1), 91–100.

[30] Kendall, R. A.; Dunning, Jr., T. H.; Harrison, R. J. *The Journal of Chemical Physics* **1992**, *96*(9), 6796–6806.

[31] Pople, J. A.; Head-Gordon, M.; Raghavachari, K. *The Journal of Chemical Physics* **1987**, *87*(10), 5968–5975.

[32] Adler, T. B.; Werner, H.-J. *The Journal of Chemical Physics* **2011**, *135*(14), 144117.

[33] Ransil, B. J. *The Journal of Chemical Physics* **1961**, *34*(6), 2109–2118.

[34] Boys, S.; Bernardi, F. *Molecular Physics* **1970**, *19*(May 2012), 553–566.

[35] Zakharenko, O.; Motiyenko, R. A.; Margules, L.; Huet, T. R. *J. Mol. Spectrosc.* **2015**, *317*, 41–46.

[36] Heger, M.; Andersen, J.; Suhm, M. A.; Wugt Larsen, R. *Phys. Chem. Chem. Phys.* **2016**, *18*(5), 3739–3745.

[37] Andersen, J.; Heimdahl, J.; Nelander, B.; Wugt Larsen, R. *The Journal of Chemical Physics* **2017**, *146*(19).

[38] Cole, W. T. S.; Fellers, R. S.; Viant, M. R.; Leforestier, C.; Saykally, R. J. *The Journal of Chemical Physics* **2015**, *143*, 154306.

[39] Andersen, J. *Ph. D. Thesis, Technical University of Denmark, Kongens Lyngby, Denmark* **2016**.

[40] Barone, V.; Biczysko, M.; Bloino, J.; Borkowska-Panek, M.; Carnimeo, I.; Panek, P. *Int. J. Quantum Chem.* **2012**, *112*, 2185–2200.

[41] Burcl, R.; Handy, N. C.; Carter, S. *Spectrochim. Acta A* **2003**, *59*, 1881.

[42] Boese, A. D.; Martin, J. M. L. *J. Phys. Chem. A* **2004**, *108*, 3085–3096.

[43] Miani, A.; Cané, E.; Palmieri, P.; Trombetti, A.; Handy, N. C. *J. Chem. Phys.* **2007**, *112*, 248.

[44] Gaw, J. F.; Willetts, A.; Green, W. H.; Handy, N. C. *In Advances in Molecular Vibrations and Collision Dynamics; Bowman, J., Ed.; JAI Press Inc. Greenwich, CT* **1991**, *1B*, 169–185.

[45] Barone, V. *J. Chem. Phys.* **2005**, *122*, 14108.

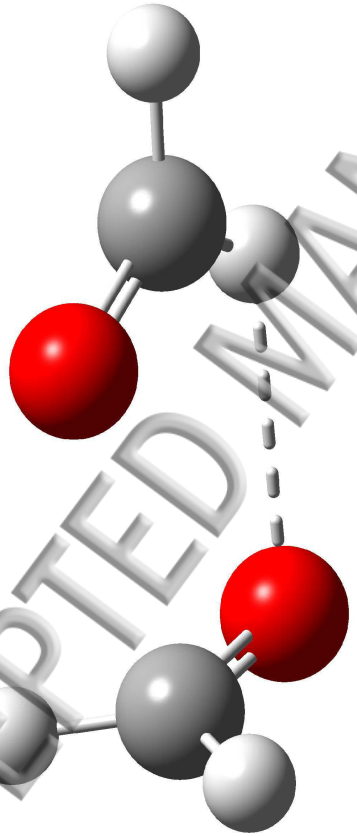

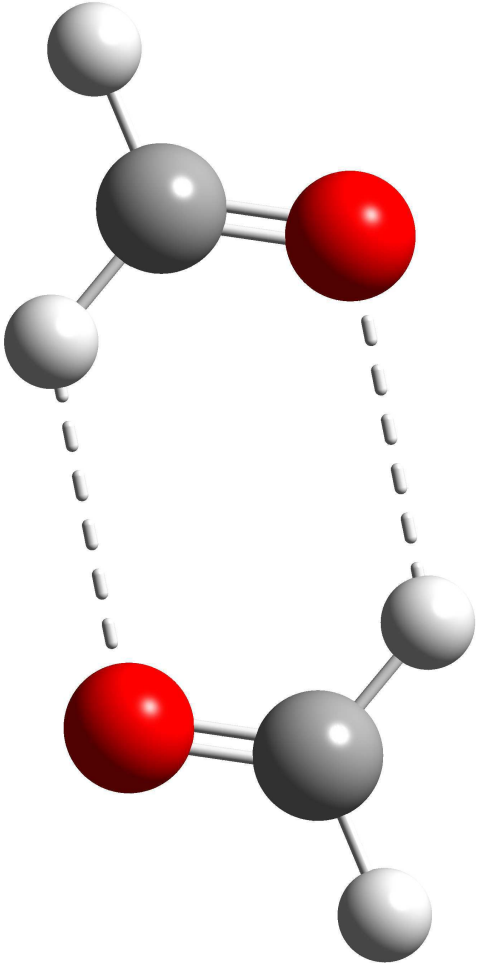

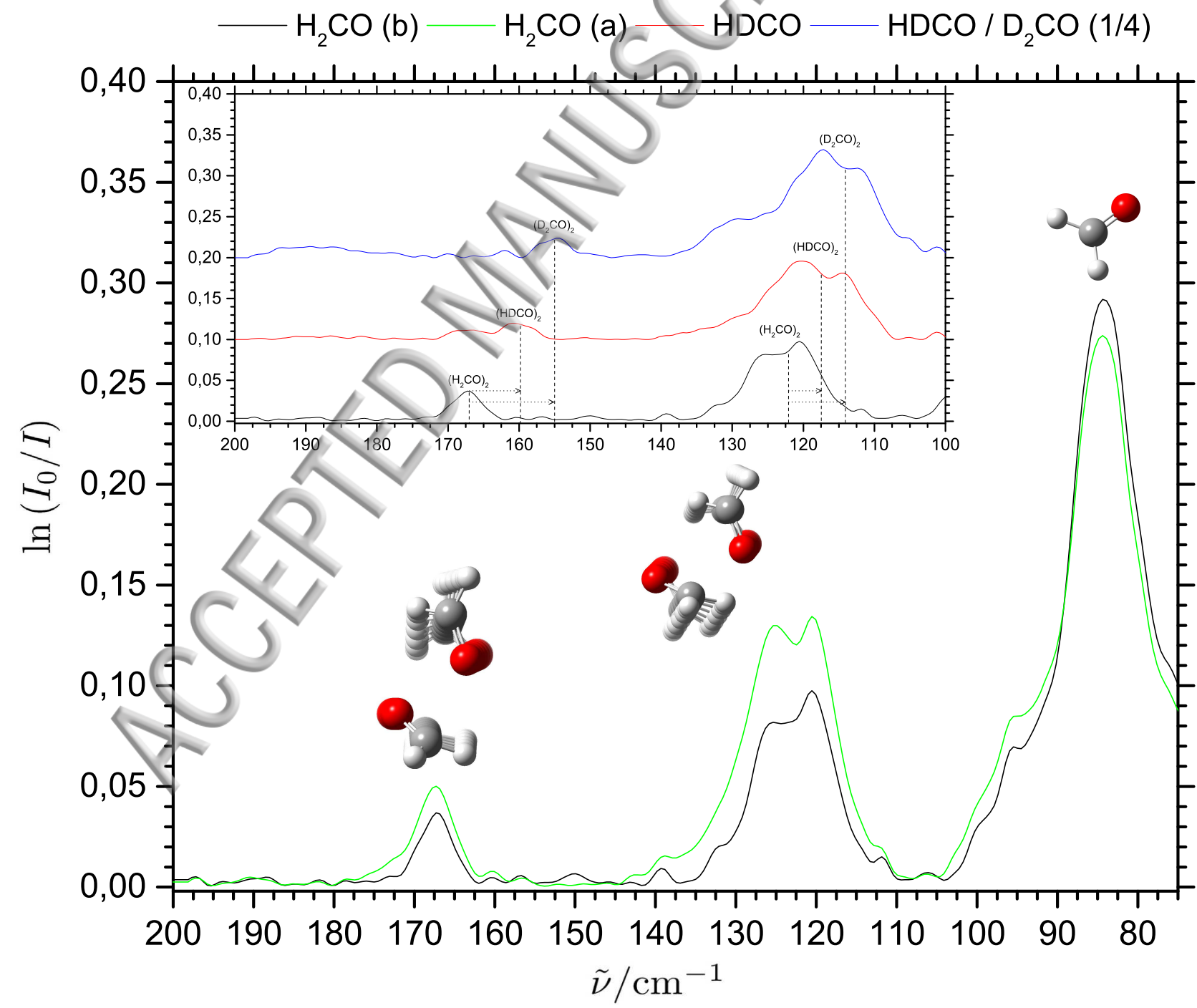
H2CO (b)
H2CO (a)
HDCO
HDCO / D2CO (1/4)
ln (I0/I)
0,40
0,35
0,30
0,25
0,20
0,15
0,10
0,05
0,00
200 190 180 170 160 150 140 130 120 110 100 90 80
ν̃/cm−1
(D2CO)2
(HDCO)2
(H2CO)2
ACCEPTED MANUSCRIPT